Fusion Engineering and Design 192 (2023) 113833

Contents lists available at ScienceDirect

Fusion Engineering and Design

journal homepage: www.elsevier.com/locate/fusengdes

Predictive simulations for plasma scenarios in the SMART tokamak

A. Mancini [a,b,*], L. Velarde [b,c], E. Viezzer [a], D.J. Cruz-Zabala [a], J.F. Rivero-Rodriguez [d], M. Garcia-Muñoz [a], L. Sanchis [e], A. Snicker [e], J. Segado-Fernandez [b], J. Garcia-Dominguez [b], J. Hidalgo-Salaverri [b,c], P. Cano-Megias [b,c], M. Toscano-Jimenez [f], the PSFT Group

[a] Department of Atomic, Molecular and Nuclear Physics, University of Seville, Seville, Spain
[b] Centro Nacional de Aceleradores (U. Sevilla, CSIC, J. de Andalucia), Sevilla, Spain
[c] Department of Energy Engineering, University of Seville, 41092 Seville, Spain
[d] United Kingdom Atomic Energy Authority, Culham Centre for Fusion Energy, Culham Science Centre, Abingdon, Oxon, OX14 3DB, UK
[e] Department of Applied Physics, Aalto University, Espoo, Finland
[f] Department of Applied Physics III, University of Seville, Spain

ARTICLE INFO

Keywords:
SMART
ASTRA
ASCOT5
FIESTA
Plasma scenarios

ABSTRACT

The SMall Aspect Ratio Tokamak (SMART) is a new spherical machine that is currently being constructed at the University of Seville (Mancini et al., 2021; Agredano-Torres et al., 2021). The operation of SMART will cover three different phases reaching an inductive plasma current (I_P) of more than 500 kA, a toroidal magnetic field (B_T) of 1 T and a pulse length of 500 ms (Mancini et al., 2021; Agredano-Torres et al., 2021). The main goal of the SMART tokamak is to study high plasma confinement regimes in a broad triangularity range ($-0.5 \leq \delta \leq 0.5$) (Doyle et al., 2021; Doyle et al., 2021). While in phase 1 the ohmic heating alone is expected to provide enough power to access the H-mode, in phase 2 and phase 3 the access to the H-mode will be ensured by applying Neutral Beam Injection (NBI) as external heating system. The NBI will consist of one injector at 25 keV and 1 MW of power. The overall design of the NBI, including injection geometry, energy and power have been optimized using the ASCOT5 code (Hirvijoki et al., 2021). The SMART scenarios have been developed with the help of the free boundary equilibrium solver code FIESTA (Cunningham, 2013) coupled to the linear time independent, rigid plasma model RZIP (Lazarus et al., 1990) to calculate the target equilibria for all the different operational phases. To assess the feasibility of those scenarios, predictive modelling needs to be included to evaluate properly the evolution of the temperatures, density profiles for both electrons and ions. To this extent, the 1.5D transport code ASTRA (Pereverzev and Yushmanov, 2002) has been used including models for the ohmic current, bootstrap current and current driven by NBI. This contribution discusses the electron and ion density and temperature profiles obtained for various scenarios for phase 1 and 2 and presents the design study of the NBI.

1. Introduction

The SMall Aspect Ratio Tokamak (SMART) is a new spherical tokamak currently being constructed and assembled at the University of Seville [1,2]. SMART will operate through three phases that differ in value of the plasma current I_p up to more than 500 kA, toroidal magnetic field B_T up to 1 T and pulse length τ up to 500 ms, see Table 1. Its versatility is the operation in single and double null configuration, and with positive and negative triangularity ($-0.5 \leq \delta \leq 0.5$ [3,4]). By phase 2, SMART will also be equipped with a Neutral Beam Injector (NBI) with a maximum power of 1 MW, to study the effects of fast-ion physics in high positive and negative triangularity scenarios. In this environment, the prediction of plasma performance of the machine is essential and can be achieved by using predictive modelling codes in order to compute the evolution of plasma profiles, such as temperature and density, for the three different phases. The aim of the paper is the description of the SMART performances in the first two phases and it is organized as follows. Section 2 will provide a general description of the SMART tokamak, while the equilibrium obtained with FIESTA [3–5] and the transport model used in ASTRA [6] will be detailed in Section 3. Phase 1 in its baseline and positive triangularity scenarios will be addressed in Section 4, while Phase 2 will be discussed in Section 5 with density and temperature profiles in 5.1 and the description of the optimization process of the NBI in 5.2. This work focuses solely in phase 1 and phase 2 in positive triangularity,

* Corresponding author at: Department of Atomic, Molecular and Nuclear Physics, University of Seville, Seville, Spain.
E-mail address: amancini@us.es (A. Mancini).

https://doi.org/10.1016/j.fusengdes.2023.113833
Received 28 October 2022; Received in revised form 31 March 2023; Accepted 17 May 2023
Available online 28 May 2023

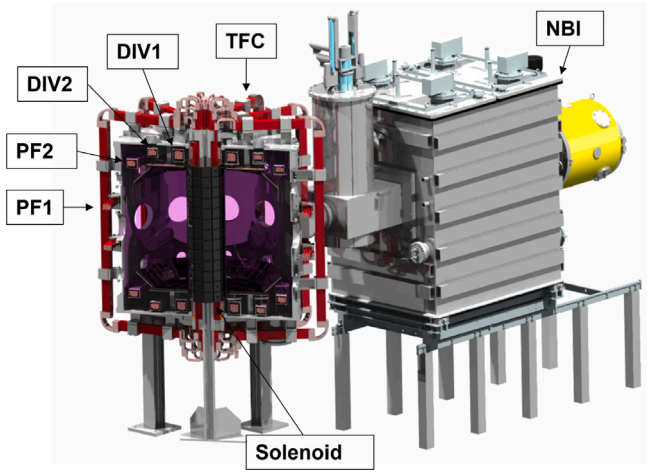

Fig. 1. Overview of the SMART tokamak together with the Neutral Beam Injector (NBI).

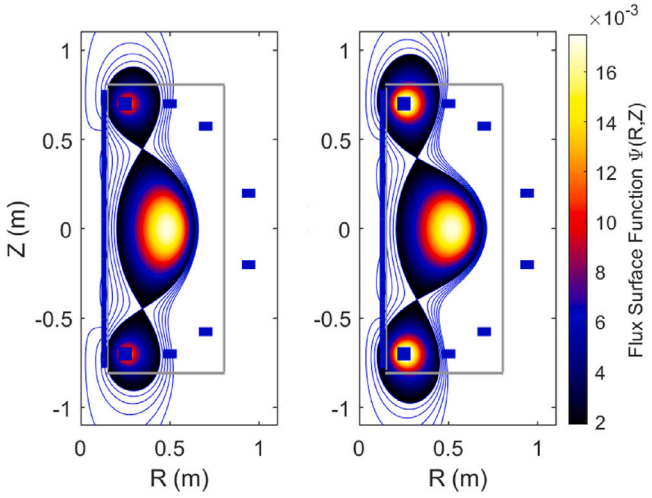

Fig. 2. Phase 1 equilibrium from FIESTA. Baseline is depicted on the left while the positive triangularity case is on the right.

while negative triangularity will be assessed in a separate work. The positive triangularity scenarios have been computed in order to assess the performance of the machine in terms of toroidal beta β_t, poloidal beta β_p, normalized beta $\beta_N = \beta_t/(I_p/(aB_T))$ and confinement time τ_E. In addition, the evaluation of those scenarios will constitute a solid base for the design of many diagnostics, and for MHD and gyrokinetics analysis, and their validity will be proven once the machine will come into operation.

2. SMART tokamak

The SMall Aspect Ratio Tokamak (SMART) is a compact spherical machine characterized by an overall height of 3 m and an overall diameter of 2 m. It is composed by an AISI 316 L stainless steel vacuum vessel having an inner wall diameter of 300 mm, outer wall diameter of 1600 mm and an inner height of 1600 mm. The vacuum vessel has an overall number of 44 circular ports and 2 rectangular ports mainly aimed for diagnostics and maintenance purposes. A set of twelve copper toroidal field coils (4 number of turns each) are capable of producing the desired toroidal magnetic field (B_T) at the major radius (R_0) of the plasma for all the operative phases (see Table 1).

Four poloidal field coils (PF1 and PF2), with 23 number of turns each, are needed for the vertical control and shaping of the plasma.

Table 1
Operative stages of the SMART tokamak.

	Phase 1	Phase 2	Phase 3
R_0 [m]	0.4	0.4	0.4
a [m]	0.25	0.25	0.25
κ	≤ 1.95	≤ 2.00	≤ 2.30
δ	± 0.4	± 0.5	± 0.5
I_P [kA]	100	200	> 500
B_T [T]	0.1	0.4	1
τ [ms]	0.100	0.150	0.500
P_{ECRH} [kW]	6 (2.45 GHz)	6 (7.5 GHz)	200
P_{NBI} [kW]	–	1000	1000

Table 2
ASTRA input model data.

	Phase 1		Phase 2	
	base	$@\delta_{max}$	base	$@\delta_{max}$
Δ_s [m]	0.059	0.067	0.035	0.032
I_P [kA]	30	30	200	200
B_T [T]	0.1	0.1	0.4	0.4
κ	1.83	1.48	1.95	1.79
δ	0.23	0.4	0.35	0.4
S_p [m^2]	5.081	5.12	6.80	6.31
V_p [m^3]	0.68	0.70	1.03	0.90
β_t	1.74	2.46	2.92	3.3
β_p	0.337	0.395	0.325	0.322
β_n	1.25	1.77	1.46	1.61

The PF1 coils are placed outside the vessel while the PF2 are placed inside (see Fig. 1). Two pairs of divertor field coils (DIV1 and DIV2 in Fig. 1), all placed inside the machine, are needed to reach the desired elongation κ and to operate the machine in single or double null configuration and in positive and negative triangularity [3,4]. The number of turns of these coils differs, being 35 for DIV1 and 23 for DIV2. A copper solenoid with 230 number of turns completes the magnetic system of the machine. SMART will be equipped with four vacuum pumps: two dry pumps of 80 m^3h^{-1} and two turbomolecular pumps of 2300 lts^{-1} designed to obtain the required level of vacuum of 10^{-8} torr with a maximum leakage of 10^{-8} mbar $\cdot$ lts^{-1}. Additional heating systems such as Electron Cyclotron Resonance Heating (ECRH) and Neutral Beam Injector (NBI) will also be installed during the operational phases of the machine. The optimization process and the parameters for the NBI are discussed in Section 5.2. Additional information are detailed in [1,2].

3. Plasma scenarios modelling

The development of the operative scenarios assume an important role in the design of tokamak devices, as they influence the operation of the machine, the assessment of the performance but also the design of several diagnostic systems which need an estimation of the profiles of electron and ion density (n_e, n_i) together with their temperature profiles (T_e, T_i). In the SMART design, the modelling of the plasma scenarios have been computed using the ASTRA code, a 1.5 D transport code which combines 2D equilibrium equations with a set of 1D transport equations [6]. The input parameters for the modelling are the major radius R_0, minor radius a, elongation κ, triangularity δ, Shafranov shift Δ_s, plasma volume V_p and plasma surface S_p, which have been computed with the FIESTA code [5,7]. The equilibrium profiles for phase 1 and phase 2 are shown in Figs. 2 and 3 with the main equilibrium parameters summarized in Table 2. The different beta (β_N, β_t and β_p) included in Table 2 have been computed with FIESTA and verified with ASTRA.

The transport simulations were carried out with ASTRA by considering a hydrogen plasma with Z_{eff} equal to 2, a Greenwald fraction (f_{GW}) of 0.4 and a GyroBohm model [8] for the transport coefficients:

$$\chi_i = C_1 \frac{a^2 T_e^{3/2}}{B_{tor}^2 \mu^2} \frac{\nabla T_e}{T_e} \tag{1}$$

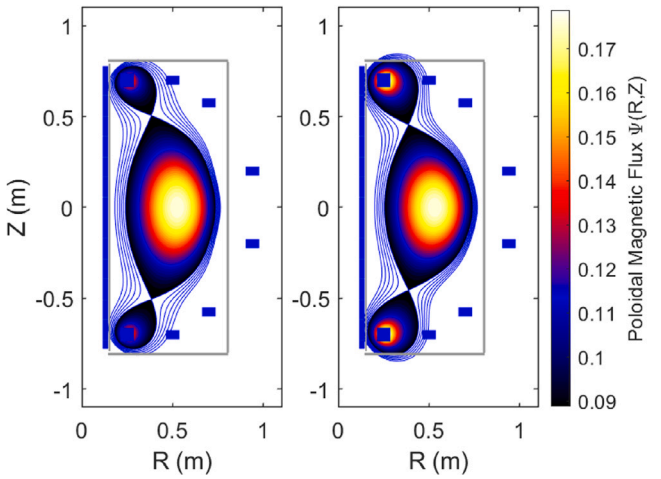

Fig. 3. Phase 2 equilibrium from FIESTA. Baseline is depicted on the left while the positive triangularity case is on the right.

$$\chi_e = 2\chi_i \tag{2}$$

$$D = C_2\chi_e \tag{3}$$

$$v = C_3 v_p V' - \frac{D}{R_0}\left(0.2\frac{R_0}{L_{Te}} + 0.1sC_4\right) \tag{4}$$

being χ_i the ion heat transport coefficient, χ_e the electron heat transport coefficient (assuming pure Ion Temperature Gradient, ITG), D the diffusion coefficient, v the convective velocity, $v_p = E_{||}/B_p$ the pinch velocity indicating with $E_{||}$ the parallel component of the electric field and B_p the poloidal component of the magnetic field. Finally $L_{Te} = T_e/\nabla T_e$ is the electron temperature gradient length scale and s the shear. The coefficients C_1, C_2, C_3 and C_4 have been chosen equal to [0.4, 0.2, 0.1, 1] to have comparable transport coefficients of machines with similar size/aspect ratio of SMART (i.e. GLOBUS-M [9] and Pegasus [10]) and to take into account also neoclassical effects. For the simulations in H-mode, χ_i has been chosen equal to 4 m^2s^{-1} with the edge transport barrier (ETB) placed at $\rho_{pol} = 0.95$ [9–11] and leaving the same approximation of the GyroBohm model for the other coefficients (see Section 5.1).

4. Phase 1 scenarios

In this section the phase 1 scenarios will be discussed both in the baseline and positive triangularity case. Simulations for phase 1 equilibria have been run with the parameters included in Table 2. Figs. 4 and 5 show the density and temperature profiles as a function of the normalized radius $\rho_{pol} = \sqrt{(\psi - \psi_b)/(\psi_b - \psi_0)}$, being ψ_b and ψ_0 the value of the poloidal flux at the separatrix and in the centre respectively.

The density increases with the triangularity both for ions and electrons. The core electron density n_{e0} increases from 0.865×10^{19} m^{-3} to 1.01×10^{19} m^{-3}, while the core ion density n_{i0} increases from of 0.7×10^{19} m^{-3} to 0.8×10^{19} m^{-3}. Temperature profiles show the same trend, with a maximum of 0.171 keV and 0.08 keV respectively for T_e and T_i in the core. The benefits of increasing the triangularity is also manifested in the reduction of the transport coefficients χ_i, χ_e and D as shown in Fig. 6.

In phase 1, no additional source of energy is used to heat the plasma apart from the intrinsically ohmic heating. The ohmic power, P_{OH}, can be estimated as [12]:

$$P_{OH}[\mathrm{MW}] = 7 \times 10^{-2}\frac{Z_{eff}B_T^2V_p}{q_a^2R_0^2T_e^{3/2}} \tag{5}$$

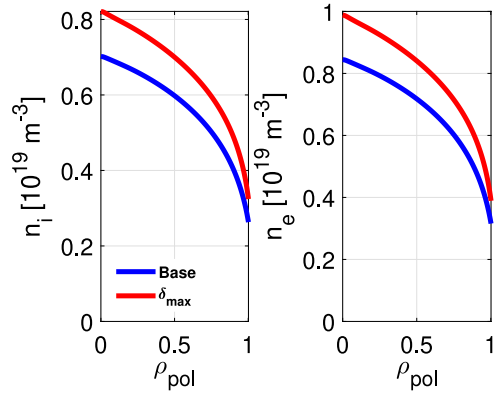

Fig. 4. n_e and n_i profiles for phase 1 in the baseline scenario and in the positive triangularity case.

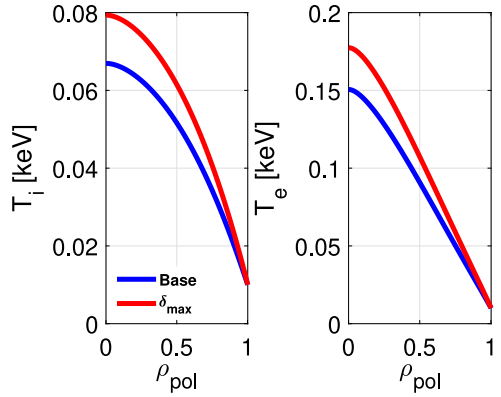

Fig. 5. T_e and T_i profiles for phase 1 in the baseline scenario and in the positive triangularity case.

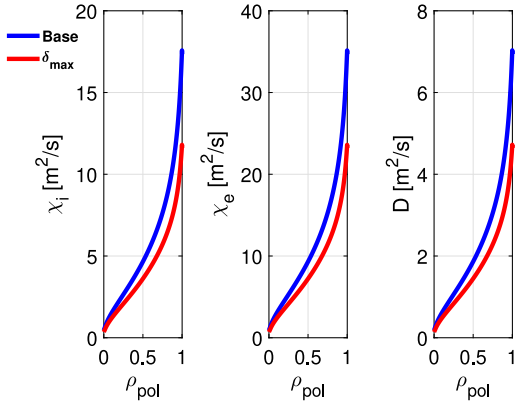

Fig. 6. χ_i, χ_e and D profiles for phase 1 in the baseline scenario and in the positive triangularity case.

where $q_a = 5\kappa a^2 B_T/RI_p$ is the safety factor at $r = a$ and T_e the average electron temperature in keV. Using this simple 0-D approximation, with the parameters included in Table 2, the ohmic power P_{OH} is 47 kW, similar to 50 kW estimated with ASTRA. The threshold power for the transition from L- to the H-mode (P_{LH}) can be evaluated with the following expression [13,14]:

$$P_{LH}[\mathrm{MW}] = 0.0488 n_{20}^{0.717} B_T^{0.803} S^{0.941} \tag{6}$$

where $S = 4\pi^2 aR\sqrt{0.5(1+k^2)}$ is the plasma surface area and n_{20} the electron average density expressed in 10^{20} unit. For phase 1, the

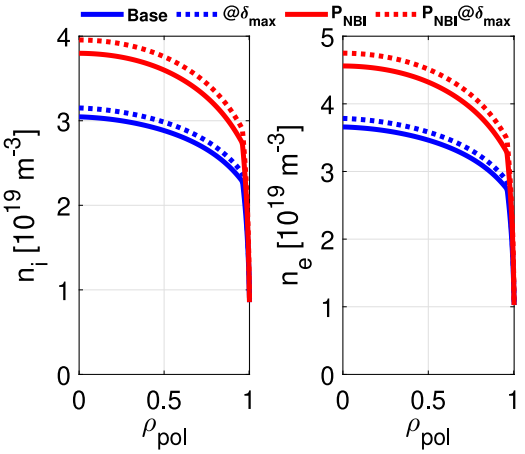

Fig. 7. Density profiles for phase 2 with and without NBI.

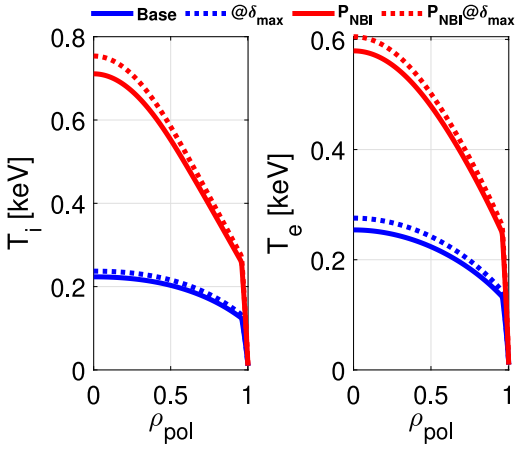

Fig. 8. Temperature profiles for phase 2 with and without NBI.

threshold power is approximately 9 kW. The radiative power P_{rad} from the plasma, approximated by the sum of the Bremsstrahlung P_{Br} and cyclotron P_{cycl} losses, can be neglected as approximately equal to 60 W. P_{Br} and P_{cycl} have been estimated with the followingexpressions [15]:

$$P_{Br}[\mathrm{W}] = \frac{Z_{eff}^2 n_i n_e T_e^{0.5}}{[7.69 \times 10^{18}]^2} V_p \tag{7}$$

$$P_{cycl}[\mathrm{W}] = 6.21 \times 10^{-22} B_T^2 n_e T_e V_p \tag{8}$$

which gives results in accordance with ASTRA simulations. Therefore, neglecting the radiative power P_{rad}, it is expected that in phase 1 SMART will achieve the ohmic H-mode ($P_{OH} \gg P_{LH}$). The energy confinement time has been approximated with the following scaling law valid at low densities and for ohmic heating [16]:

$$\tau_E[\mathrm{s}] = 0.07 n_{20} a R_0^2 q_{cyl} \tag{9}$$

where $q_{cyl} = 5a^2 B_T / I_p R$ the cylindrical safety factor. For phase 1, an energy confinement time of 0.33 ms is expected while ASTRA predicts 0.22 ms, slightly lower but of the same order of magnitude. The bootstrap current fraction f_{bs} is expected to increase with the triangularity δ from 14.3% to 15.1% as there is a small increase in β_p, see Table 2.

5. Phase 2 scenarios

5.1. ASTRA results

ASTRA simulations have been carried out in order to determine the profiles of density and temperature in phase 2 with and without the NBI. The parameters of the NBI used for the ASTRA simulations are the injected power (P_{NBI}) of 1 MW and energy (E_0) of 25 keV as described in Section 5.2. Only the NBI heating has been included in the simulations. No ECRH heating has been considered as it will only be used for pre-ionization during the plasma start-up. The baseline case has been compared with the extreme positive triangularity, even though the two configurations differ slightly (see Table 2). Figs. 7 and 8 show the density and temperature profiles in phase 2 where the blue curves represents the scenarios without NBI, and the red ones with the NBI. Dotted curves in both cases represent the scenarios in the highest positive triangularity case. With the NBI a rise in both density and temperature is expected. n_{e0} and n_{i0} will increase up to 4.7×10^{19} m^{-3} and 3.8×10^{19} m^{-3}. No big difference is expected between the baseline and the extreme positive triangularity case, as the difference in triangularity for those two cases is 0.1.

A large increase is expected in the electron and ion temperature. T_e and T_i will increase up to 0.56 keV and 0.7 keV respectively in the baseline case. In the case of extreme positive triangularity, the ion temperature will be slightly higher up to 0.75 keV and the electron temperature up to 0.6 keV. Scenarios with NBI will enhance the β parameters. In the baseline case, the β_t will rise up to 8.23%, β_p up to 0.7 and β_N up to 4.1, compared to the values reached in phase 1 (see Table 2). In the extreme positive case β_t will rise up to 9.1%, β_p of 0.69 and β_N up to 4.44. Moreover, ASTRA results foresee a bootstrap current fraction that increase from $f_{bs} \approx 15\%$ in phase 1 to $f_{bs} \approx 37\%$ in phase 2 ($I_{bs} \approx 66$ kA), with a current fraction induced from the NBI (f_{CD}) of almost 15% which corresponds to an induced current $I_{CD} \approx$ 30 kA, in line with the results of GLOBUS-M [17].

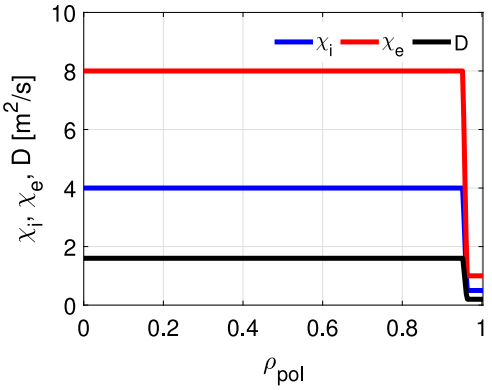

Fig. 9. Transport coefficients with the ETB located at $\rho_{pol} = 0.95$.

ASTRA simulations predict that the total beam power P_{CD} is approximately 0.7 MW high enough to overcome P_{LH}, see formula (6), which is approximately 90 kW. The radiative power can be neglected as in phase 1. In fact, using the formulas (7) and (8), the radiative power can be estimated to almost 2.2 kW. Therefore it is expected that in phase 2 with the NBI, SMART will achieve the H-mode as $P_{CD} \gg P_{LH}$. In addition without the NBI, the ohmic power (P_{OH}), evaluated with the formula (5), is approximately 0.22 MW similar to the 0.27 MW obtained with ASTRA. As the ohmic power is higher than the threshold power it is likely to expect that SMART will achieve in a H-mode regime also without the NBI. This justifies the approximation of using the transport coefficients with the profiles shown in Fig. 9 and described in Section 3.

As the operation will be in H-mode, the confinement time τ_E can be estimated with the ITER IPB(y,2) scaling law [18]:

$$\tau_E[\mathrm{s}] = 0.145 \frac{I_P^{0.93} R_0^{1.39} a^{0.58} k^{0.78} n_{20}^{0.41} B_T^{0.15} M^{0.19}}{P_H^{0.69}} \quad (10)$$

where $P_H = P_{NBI}$ is the external heating power. For phase 2 we get a confinement time of 6.5 ms slightly lower but of the same order of magnitude of the one computed by ASTRA, 10 ms. A better estimation of the confinement time τ_E is obtained when considering a NSTX-GyroBohm scaling law valid for spherical tokamaks [19]:

$$\tau_E[\mathrm{s}] = 0.21 \frac{I_p^{0.054} B_T^{0.91} R_0^{2.14}}{n_e^{0.05} P_H^{0.38}} \quad (11)$$

which gives a τ_E of almost 9 ms, in line with the ASTRA results.

5.2. NBI design and optimization

To ensure H-mode in phase 2, 1 MW of Neutral Beam Injection (NBI) will be applied to positive-triangularity SMART plasmas. Beam height and width have been determined scaling NBIs of similar machines in size of SMART, such us Globus-M. The preliminary dimensions of the grid beams considered in the simulations are height and width of 30 cm and 33 cm respectively. The main parameters of the NBI have been optimized through the Monte-Carlo orbit-following code ASCOT5 [20], using the wall geometry and the magnetic equilibrium calculated with FIESTA (see Section 3) and the temperature and density profiles obtained with ASTRA without external heating, see Section 5.1. The optimization of the main NBI parameters has been performed with an iterative process, analysing the confinement of different particles injected at the separatrix ($r = 0.75$ m and $z = 0$ m) and ionized inside the plasma. Here, the optimization of the injection geometry is presented, performed setting the NBI main beam energy, E_0, to 25 keV. This has been considered as the best choice for phase 2 according to previous analysis, and matching the energy observed in other similar machines [9]. The energy of the beam is limited on one hand by the gyroradius of the resulting particles, that increases with energy ($r_L = mv_\perp/qB \propto E_0/B$), and by the orbit drifts, thus affecting fast-ion losses. On the other hand, the higher the energy, the lower the cross-section of the global ionization processes between the injected neutrals and the thermal plasma [21], increasing the shine-through (i.e., the percentage of particles that travel through the plasma without getting ionized), and thus, decreasing the total efficiency. Therefore, the two main parameters employed to optimize the NBI geometry and energy are the prompt losses (i.e., particles that are lost before completing a toroidal period) and the shine-through. Moreover, a 25 keV injection energy provides a super-Alfvénic fast-ion distribution, as the Alfvén velocity at $\rho_{pol} = 0.5$ is $v_A \sim 1.6 \times 10^6$ m/s, while the velocity corresponding to the main injection energy is $v = 2.2 \times 10^6$ m/s, making it possible to drive unstable a wide variety of Alfvén Eigenmodes, enabling to study their behaviour as a function of plasma shape and triangularity. Higher injection energies, up to 35 keV, will also be considered during the optimization process.

In order to optimize the injection configurations, the fast-ion birth distribution has been modelled with a set of 10^6 markers (high enough to achieve good statistics, according to previous analysis), whose orbits are followed for 1 ms. The different sets of markers have been generated with the BBNBI code [22], by varying the tangency radius of the beam centre line, as shown in Fig. 10. Then, by means of the ASCOT5 code, the ionized particles have been followed in a collisionless and MHD-quiescent environment, in order to calculate the percentages of prompt losses (as mentioned, particles lost before completing a toroidal period, and thus, not affected by Coulomb collisions). The selected simulation time is sufficient to account for the prompt losses. The shine-through has also been calculated for each of the 9 cases studied, with the aim to minimize the total amount of particles that are lost.

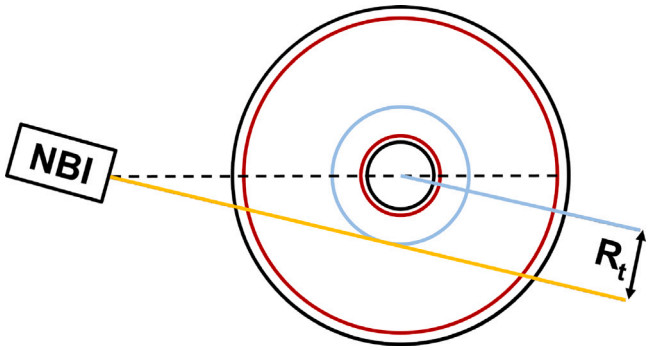

Fig. 10. Sketch of the toroidal view of the SMART NBI configuration. The black circles represent the vessel walls and the red ones the toroidal section of the separatrix. The yellow line represents the beamline. The perpendicular distance from the beam to the centre of the device is represented by the blue circle and line, indicating the tangency radius, R_t.

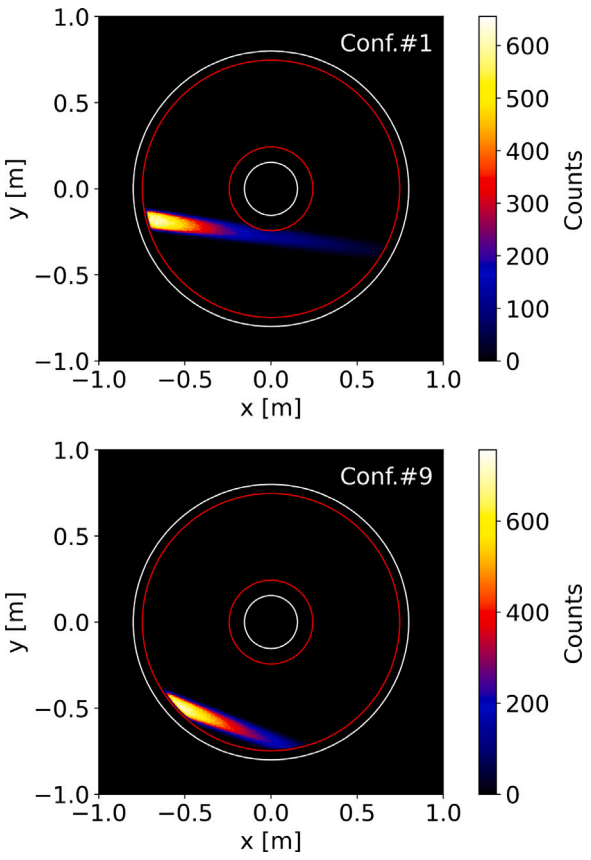

Fig. 11. NBI birth distribution in the toroidal projection for the most extreme configurations, #1 (up) and #9 (down).

The results for the different configurations studied by varying the chosen optimization parameter, R_t, are shown in Fig. 12. As the plasma inner and outer radius is located at 0.243 m and 0.747 m, R_t has been modified from 0.280 m to 0.735 m. The toroidal view of the birth distribution of the particles generated with these two extreme configurations are shown in Fig. 11.

The minimum total amount of losses is provided by configurations #3 and #4, see Fig. 12. The rise in the shine-through with R_t is explained considering that, as the tangency radius is increased, the beam travels a shorter path through the plasma, in a region with lower density. On the contrary, increasing the tangency radius, the beam aligns with the magnetic field lines, decreasing the prompt losses to

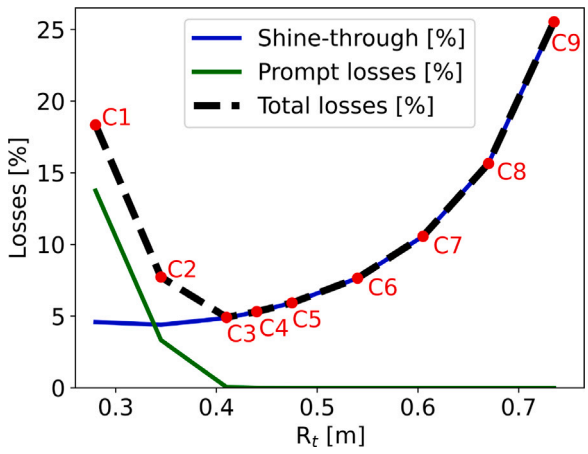

Fig. 12. Evolution of the resulting losses for the different configurations (red circles) studied for the NBI system.

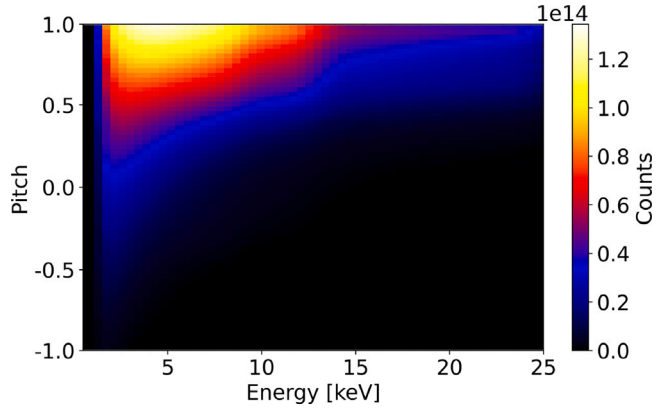

Fig. 13. Slowing down distribution for the optimum configuration, #4, in pitch-energy.

a negligible level. Hence, configurations from #5 to #9 should be discarded, as the shine-through is too high, as well as configurations #1 and #2, due to their higher result in prompt losses in comparison to the others.

As configurations #3 and #4 show similar results, the shine-through and the prompt losses have been computed at higher injection energies, up to 35 keV, for both geometries. This criteria has been chosen in order to assess their performance in the possible case of an increase in the energy of the beam in the future [23], which would be performed without changing the injection geometry of the NBI. 35 keV is set as the maximum permitted injection energy, as it allows maintaining the shine-through below 10% with the current plasma profiles. The results in Table 3 show that, as the energy increases, the prompt losses in configuration #3 rise rapidly. The shine-through, on the contrary, increases for both configurations, and its absolute value is comparable.

This evolution of the prompt losses with the energy has led to choose configuration #4 as the optimum one, showing that the injection energy of the NBI system could be increased in the future if desired, and the prompt losses would stay in an admissible range, while preserving an acceptable evolution of the shine-through fraction, always kept below 10%.

The slowing down distribution for configuration #4 and a 25 keV injection energy has also been analysed. For this simulation, the injected particles are allowed to interact with the bulk plasma via Coulomb collisions for 1 s, which is found sufficient for most of the fast-ion distribution to thermalize. The markers are stopped when they reach either the selected thermal limit of 1 keV, or the maximum simulation

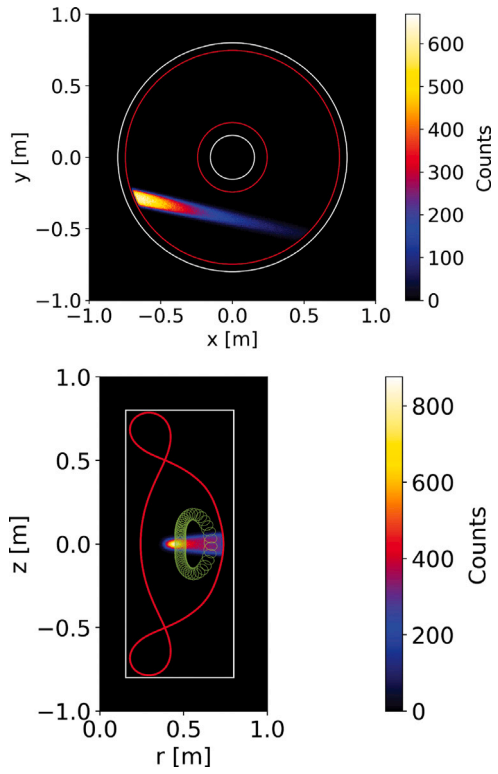

Fig. 14. Birth distribution of the particles generated with the optimized configuration (#4). Toroidal (up) and poloidal (down) projections. The latter includes a typical confined orbit.

Table 3
Resulting losses for configurations #3 and #4, and different injection energies.

ID	Energy	Shine-through	Prompt losses	Total losses
3	25 keV	4.9%	0.1%	5.0%
	30 keV	6.9%	0.4%	7.3%
	35 keV	9.0%	1.1%	10.1%
4	25 keV	5.3%	**0.0** %	5.3%
	30 keV	7.4%	**0.1** %	7.5%
	35 keV	9.6%	**0.5** %	10.1%

time. As shown in Fig. 13, most of the particles have a pitch angle above 0.9, meaning that they will describe passing orbits. This is desirable in order to reduce possible losses due to the drift of trapped orbits, and results in a better confinement of the beam particles. Hence, the birth distribution for the selected configuration (#4) is shown in Fig. 14, where an example of a passing orbit has been plotted in the poloidal projection of the distribution.

6. Conclusions

Reference scenarios for the SMART tokamak have been computed with the 1.5D transport code ASTRA coupled with FIESTA to predict the density and temperature profiles needed primarily for the assessment of the performances of the machine. Only the baseline and maximum positive triangularity scenarios have been considered for phase 1 and phase 2. In phase 1 the parameters chosen here suggest that the machine will access the H-mode with a maximum n_{e0} and n_{i0} of 1×10^{19} m^{-3} and 0.8×10^{19} m^{-3}. Maximum temperature T_{e0} and T_{i0} of 0.171 keV and 0.080 keV will be achieved with a maximum confinement energy time τ_E of 0.2 ms, lower than the one estimated with the confinement scaling law for ohmic heating but of the same order of magnitude. Phase 2 will be equipped with a Neutral Beam Injector whose characteristics have been presented together with the optimization of its parameters,

in particular energy and injection geometry. The best configuration has been determined, opening the possibility of increasing the NBI energy without changing the injection geometry in the future. ASTRA simulations for phase 2 predict that SMART will access H-mode with and without NBI as both the Ohmic Power (P_{OH}) and the NBI coupled power (P_{CD}) are sufficiently higher than the threshold power (P_{LH}) as long as the experiments will confirm that the radiative power losses will be negligible. Core densities up to 4.65×10^{19} m^{-3} will be reached with a core temperature of 0.75 keV. Beta normalized β_N will increase up to 4.4 with a toroidal β_t up to 9%. A bootstrap current fraction of f_{bs} of 37% will be reached and a NBI current drive fraction f_{CD} of 15% is expected. Negative triangularity profiles will be assessed in a separate work, exploring also the phase 3 scenario.

Declaration of competing interest

The authors declare that they have no known competing financial interests or personal relationships that could have appeared to influence the work reported in this paper.

Data availability

Data will be made available on request

Acknowledgements

This work received funding from the Fondo Europeo de Desarollo Regional (FEDER) by the European Commission under grant agreement numbers IE17-5670 and US-15570. The authors gratefully acknowledge the financial support of the European Research Council (ERC) under the European Union's Horizon 2020 research and innovation programme (grant agreement No. 805162).

References

[1] A. Mancini, et al., Mechanical and electromagnetic design of the vacuum vessel of the SMART tokamak, Fusion Eng. Des. 171 (2021).
[2] M. Agredano-Torres, J.L. Garcia-Sanchez, A. Mancini, et al., Coils and power supplies design for the SMART tokamak, Fusion Eng. Des. 168 (2021).
[3] S.J. Doyle, D. Lopez-Aires, A. Mancini, et al., Magnetic equilibrium design for the SMART tokamak, Fusion Eng. Des. 171 (2021).
[4] S.J. Doyle, A. Mancini, et al., Single and double null equilibria in the SMART tokamak, Plasma Res. Express 3 (2021).
[5] G. Cunningham, High performance plasma vertical position control system for upgraded MAST, Fusion Eng. Des. 88 (2013) 3238–3247.
[6] G.V. Pereverzev, P.N. Yushmanov, ASTRA automated system for transport analysis, IPP Rep. (2002).
[7] E.A. Lazarus, J.B. Lister, G.H. Neilson, Control of the vertical instability in tokamaks, Nucl. Fusion 30 (1990).
[8] A. Taroni, et al., Global and local energy confinement properties of simple transport coefficients of the bohm type, Plasma Phys. Control. 36 (1994) 1629.
[9] I.Y. Senichenkov, et al., Simulation of L and H regimes for spherical tokamak Globus-M with ASTRA transport code, in: 35th EPS Conference on Plasma Physics, 2008.
[10] K.E. Thome, et al., High confinement mode and edge localized mode characteristics in a near-unity aspect ratio tokamak, Phys. Rev. Lett. 116 (2016).
[11] E. Viezzer, et al., Ion heat transport dynamics during edge localized mode cycles at ASDEX upgrade, Nucl. Fusion 58 (2018).
[12] W.M. Stacey, Fusion: An Introduction to the Physics and Technology of Magnetic Confinement Fusion, 2010.
[13] K.E. Thome, et al., H-mode plasmas at very low aspect ratio on the pegasus toroidal experiment, Nucl. Fusion 57 (2016) 022018.
[14] Y.R. Martin, et al., Power requirement for accessing the H-mode in ITER, J. Phys. Conf. Ser. 123 (2008) 012033.
[15] NRL, NRL plasma formulary, NRL/PU/6790–18-640, 2018.
[16] W.M. Stacey, Fusion Plasma Physics, 2012.
[17] P.B. Shchegolev, et al., NBI for heating and current drive in spherical tokamak Globus-M,-M2, in: 43rd EPS Conference on Plasma Physics, 2016.
[18] ITER-Physics Expert Group on Confinement and Transport, et al., Chapter 2, Nucl. Fusion 39 (1999).
[19] P.F. Buxton, et al., On the energy confinement time in spherical tokamaks: Implications for the design of pilot plants and fusion reactors, Plasma Phys. Control. Fusion 61 (2019).
[20] E. Hirvijoki, et al., ASCOT: Solving the kinetic equation of minority particle species in tokamak plasmas, Comput. Phys. Comm. 185 (2014) 1310–1321.
[21] A.C. Riviere, Penetration of fast hydrogen atoms into a fusion reactor plasma, Nucl. Fusion 11 (1971) 363–369.
[22] O. Asunta, et al., Modelling neutral beams in fusion devices: Beamlet-based model for fast particle simulations, Comput. Phys. Comm. 188 (2015) 33–46.
[23] A.Y. Telnova, et al., New 50 keV neutral beam injector for the Globus-M2 spherical tokamak, J. Phys. Conf. Ser. 1400 (2019).